Influence of Fiber Orientation on the Elastic Limit Tensile Stress of UHPFRC

Jian Zhan (corresponding author) – Doctoral student, EPFL – École Polytechnique Fédérale de Lausanne, Laboratory for Maintenance and Safety of Structures, Lausanne, Switzerland, Email: jian.zhan@epfl.ch

Emmanuel Denarié, Ph.D. – Senior Scientist, EPFL – École Polytechnique Fédérale de Lausanne, Laboratory for Maintenance and Safety of Structures, Lausanne, Switzerland, Email: emmanuel.denarie@epfl.ch

Eugen Brühwiler, Ph.D. – Professor, EPFL – École Polytechnique Fédérale de Lausanne, Laboratory for Maintenance and Safety of Structures, Lausanne, Switzerland, Email: eugen.bruehwiler@epfl.ch

Abstract

The elastic limit tensile stress of UHPFRC is governed by contributions of the cementitious matrix and the fibrous skeleton. This paper finds that fiber orientation has significant influence on the matrix tensile strength of UHPFRC, while this is not considered in current estimation of elastic limit tensile stress. An original model relating fiber orientation to the elastic limit tensile stress is proposed. Uniaxial tensile tests have been conducted on ten dumbbell-shaped specimens, whose local fiber volume and orientation are determined using a magnetic probe before testing. Based on the results of local fiber distribution, the influence of fiber orientation on the elastic limit tensile stress is discussed, showing that the proposed model estimates well the elastic limit tensile stress of UHPFRC.

Keywords: UHPFRC, Elastic limit tensile stress, Uniaxial tensile test, Fiber orientation, Model

1. Introduction

Ultra-high Performance Fiber Reinforced Cementitious Composites (UHPFRC) present remarkable mechanical properties and a dense matrix. A commonly accepted definition of UHPFRC in terms of material properties is: (1) average elastic limit tensile stress f_{Ute}, hereafter called elastic limit, larger than 7 MPa, (2) average tensile strength f_{Utu} from 8 to 14 MPa, (3) strain hardening deformation from 1 to 5‰, (4) 5%-fractile characteristic value of compressive strength larger than 120 MPa.

As shown in Figure 1, the elastic limit f_{Ute} is higher than the matrix tensile strength σ_{mu} and lies at the transition region from the elastic behavior to strain-hardening behavior. Beyond the elastic limit, material properties of UHPFRC progressively degrade, impairing properties relevant for serviceability of structures. However, knowledge on the mechanisms governing the elastic limit of UHPFRC is scarce.

This paper proposes an original model relating fiber orientation to the elastic limit of UHPFRC. Uniaxial tensile tests are conducted on ten dumbbell-shaped specimens, whose local fiber distribution (volume and orientation) is measured before testing. The elastic limit is determined by

means of the secant-modulus drop method (Hafiz and Denarié; Denarié et al.). Based on the experimental results from the present study and a reference, the influence of fiber orientation and volume on the elastic limit is discussed.

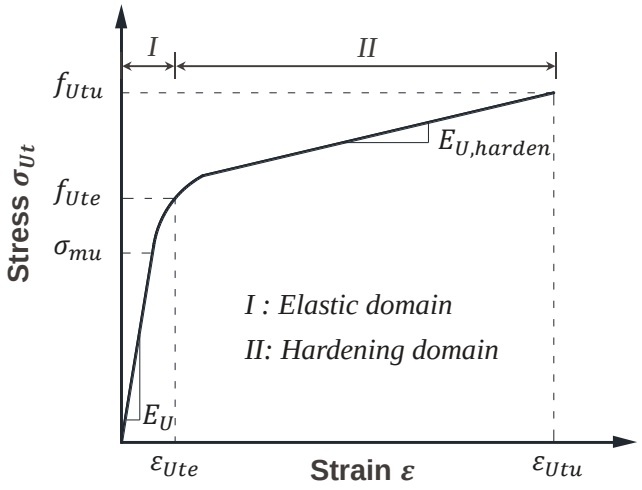

Figure 1 Typical stress-strain curve of strain-hardening UHPFRC

2. Influence of Fiber Orientation on Elastic Limit

2.1 Background

The tensile strength of UHPFRC f_{Utu} can be estimated with equation (1) (Naaman; Bastien-Masse et al.).

$$f_{Utu} = \mu_0 \mu_1 V_f \tau_f \frac{l_f}{d_f} \quad (1a)$$

$$\mu_0 = n_f \frac{A_f}{V_f} \quad (1b)$$

Where μ_0 is the fiber orientation coefficient; μ_1 is the fiber efficiency coefficient; V_f is the fiber volume fraction; τ_f is the maximum fiber pull-out strength; l_f/d_f and A_f respectively denote the aspect ratio and sectional area of a fiber; n_f is the number of fibers crossing a unit area.

Naaman proposed the following model (Naaman) to estimate the elastic limit.

$$f_{Ute} = \sigma_{mu}(1 - V_f) + \alpha \tau V_f \frac{l_f}{d_f} \quad (2a)$$

$$\alpha = \alpha_1 \alpha_2 \alpha_3 \quad (2b)$$

Where σ_{mu} is the matrix tensile strength; α_1 is the average contribution of bond at onset of matrix cracking; α_2 is the efficiency factor of fiber orientation in the uncracked state of the composite; α_3 is the reduction coefficient of bond strength at the fiber-matrix interface; τ is the equivalent bond strength at the fiber-matrix interface; V_f and $\frac{l_f}{d_f}$ are the same as in equation (1).

In equation (2), the first and second terms respectively account for the contributions of matrix and fibers, in which the matrix tensile strength σ_{mu} is fixed and assumed not to be influenced by the fibers. However, the apparent matrix tensile strength of UHPFRC is strongly influenced by the fiber orientation when it significantly deviates from the direction of principal stresses. Using the same material, the ratio of σ_{mu} between two UHPFRC specimens could be greater than 3 (Maya

Duque and Graybeal; Nunes et al.; Oesterlee). Thus, equation (2) does not consider all effects related to the elastic limit of UHPFRC.

2.2 Proposed model

Table 1 summarizes the tensile test results of UHPFRC from three research works (Nunes et al.; Shen and Brühwiler; Maya Duque and Graybeal). The average fiber orientation $\mu_{0,y}$, elastic limit f_{Ute} and tensile strength f_{Utu} are experimentally determined, in which f_{Ute} is determined using the modulus-drop method (Denarié et al.; Hafiz and Denarié). The fiber efficiency coefficient μ_1 is determined using the relation between $\mu_{0,y}$ and μ_1 (Bastien-Masse et al.), y being the direction of principal stresses. The maximum fiber pull-out strength τ_f is calculated using equation (1a). The maximum theoretical tensile strength $f_{Ut}^*=\tau_f * \sum V_{fi} l_{fi}/d_{fi}$ is defined and the elastic limits from the three research works using different UHPFRC mixes are normalized to $r_{Ut} = f_{Ute}/f_{Ut}^*$. Values of $\sum V_{fi} l_{fi}/d_{fi}$ are 1.8 and 0.9 for specimens with fiber content of 3.0% and 1.5% in (Nunes et al.), while 1.27 and 2.83 for specimens in (Maya Duque and Graybeal) and (Shen and Brühwiler), respectively.

Figure 2 shows the results of $\mu_{0,y}$ and f_{Ute} from three research. When $\mu_{0,y}$ is between around 0.28 and 0.875, a linear relation can be found between $\mu_{0,y}$ and f_{Ute}. According to (Martinie and Roussel; Oesterlee; Bastien-Masse et al.), when $\mu_{0,y}$ is higher than 0.875, fibers can be regarded as fully aligned. Besides, when fibers are mostly perpendicular to principal stresses, the fibers act like round or elliptic defects. Consequently, with the decrease of $\mu_{0,y}$ to very low values, fracture mechanics mechanisms become more prominent and the linear relation is no longer applicable.

Furthermore, the results of fiber orientation $\mu_{0,y}$ and the normalized elastic limit r_{Ut} are shown in Figure 3. A linear equation is obtained between $\mu_{0,y}$ and r_{Ut} with a correlation of 0.83. Finally, the relation between $\mu_{0,y}$ and f_{Ute} is proposed as follows:

- $0.875 \leq \mu_{0,y} \leq 1.0$: $r_{Ut} = 0.603$. Elastic limit is not influenced by $\mu_{0,y}$.
- $0.28 \leq \mu_{0,y} \leq 0.875$: $r_{Ut} = 0.676\mu_{0,y} + 0.011$. Elastic limit grows with $\mu_{0,y}$-increase.
- $\mu_{0,y} \leq 0.28$: $r_{Ut} = 0.20$. According to linear elastic fracture mechanics, a round or elliptic defect in an infinite plate leads to a stress concentration factor of larger than 3 (Oesterlee; Inglis). r_{Ut}=0.2, corresponding to 0.603 divided by 3, is thus taken as the lower limit.
- $f_{Ute} = r_{Ut} * f_{Ut}^*$.

Table 1 Summary of tensile test results

Item	Casting method	Test	V_f (%)	$\mu_{0,y}$	f_{Ute} (MPa)	f_{Utu} (MPa)	μ_1	τ_f (MPa)	f_{Ute}/f_{Ut}^*
(Nunes et al.)	Magnetically oriented to Y direction	1	3.0	0.81	9.65	16.47	1.00	11.3	0.47
		2		0.77	11.63	16.41	1.00	11.8	0.55
	Not oriented	3		0.49	5.40	7.16	0.91	8.9	0.34
		4		0.51	4.63	7.19	0.91	8.6	0.30
	Magnetically oriented to X direction	5		0.39	3.37	3.67	0.86	6.1	0.31
		6		0.28	2.88	3.18	0.72	8.7	0.18
	Magnetically oriented to Y direction	7	1.5	0.89	6.39	10.81	1.00	13.5	0.53
		8		0.83	5.67	7.7	1.00	10.3	0.61
	Not oriented	9		0.65	2.31	4.12	0.97	7.3	0.35

	Magnetically oriented to X direction	10		0.27	1.91	1.91	0.70	11.2	0.19
		11		0.18	1.43	1.43	0.47	18.9	0.08
(Maya Duque and Graybeal)	Extracted from slabs cast from one end, cutting angles are with respect to flow direction.	90° set	2.0	0.37	5.10	6.60	0.84	16.7	0.24
		45° set		0.57	7.00	7.90	0.93	11.8	0.47
		0° set		0.72	9.90	13.00	1.00	14.3	0.55
(Shen and Brühwiler)	Extracted from a slab, fresh UHPFRC poured in the formwork center to fill the formwork.	T1-1	3.8	0.68	9.96	12.85	0.98	6.8	0.54
		T1-2		0.62	9.87	11.55	0.95	6.9	0.50
		T1-3		0.53	8.20	9.62	0.92	7.0	0.43
		T1-4		0.53	8.62	9.80	0.92	7.1	0.42
		T1-5		0.52	8.10	9.49	0.91	7.1	0.41

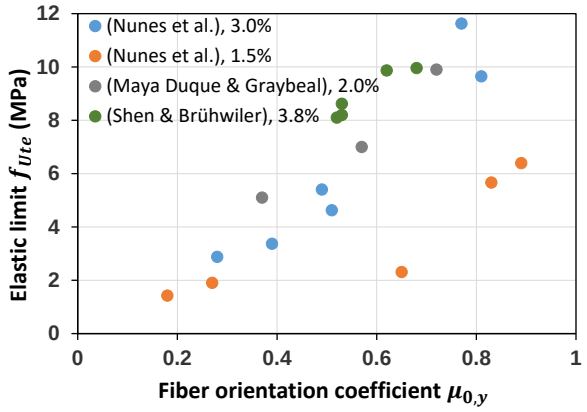

Figure 2 Results of fiber orientation and elastic limit

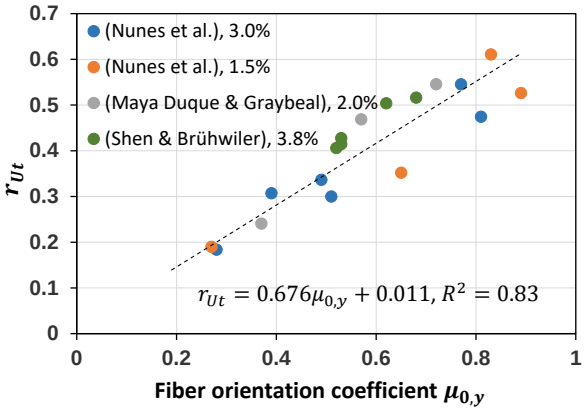

Figure 3 Results of fiber orientation and r_{Ut}

3. Experimental campaign

The UHPFRC product "Holcim 707" is employed in this research. The fiber dosage is 3.42% in volume. The fiber length and diameter are 13 mm and 0.16 mm, respectively. To prepare 1 m^3 UHPFRC of this product, the quantity of premix, steel fibers, superplasticizer (total) and water are 1978 kg, 268.0 kg, 29.2 kg and 175.8 kg, respectively.

The dimensions of the dumbbell-shaped specimen are shown in Figure 4. Ten specimens (QS-1 to 10) are cast individually in the formwork from one end to the other. Specimens are demolded at the age of 2 days and stored under 100% RH for one week. Afterward, specimens are stored in the laboratory for more than 3 months until testing when more than 95% final properties of UHPFRC are obtained (Habel et al.). The ambiant temperature is always 20 ± 5°C. Before testing, the local fiber volume and orientation on the sheathed and casting sides are determined using a magnetic probe. Details of this method can be found in (Shen and Brühwiler).

The tensile tests are carried out in a servo-hydraulic machine (Figure 4). The specimen is installed in the machine using the "gluing without bonding" approach (Helbling and Brühwiler). The specimen ends are fixed in the machine without any hinge. Using the stroke-controlled mode, the displacement rate is 0.05 mm/min. The linear variable displacement transducers (LVDT), digital image correlation (DIC) and acoustic emission (AE) are used as measurement methods. The recording frequency of LVDT, DIC and AE are 10 Hz, 2 Hz and 10 MHz respectively.

Specimens QS-1 to 3 are loaded until failure, while QS-4 to 10 are loaded to the strain of 1.5‰ and then unloaded.

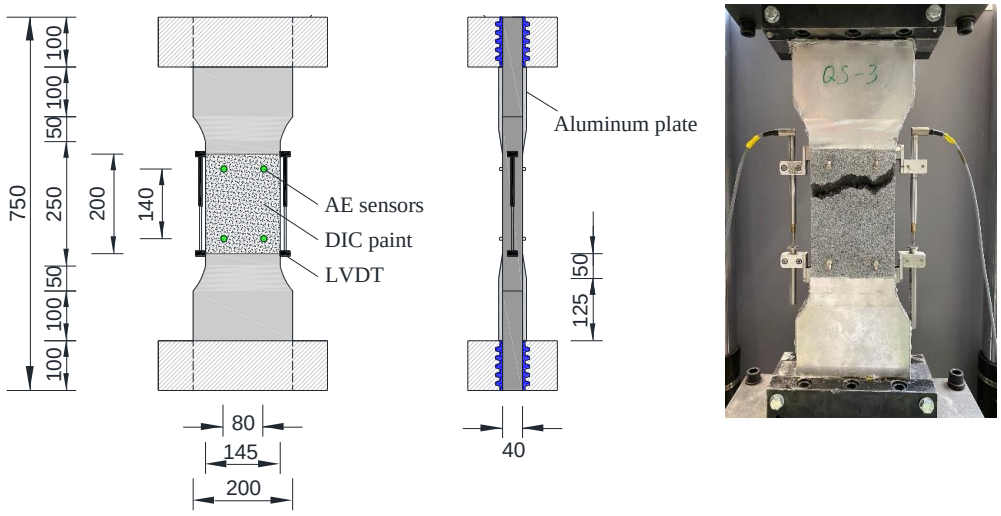

Figure 4 Specimen and test setup

4. Results and Discussion

Regarding specimens QS-1 to 10, the results of local fiber volume V_f and orientation $\mu_{0,y}$ are shown in Figures 5 and 6, respectively. The results of average local fiber distribution and tensile features are summarized in Table 2. Because the same UHPFRC matrix and similar fibers (length of 13 mm, diameter of 0.175 mm) are used, the results of (Shen and Brühwiler) are included in Table 2 and the average τ_f of 7 MPa obtained from (Shen and Brühwiler) (Table 1) is used to calculate the theoretical elastic limit $f_{Ute,cal}$ and tensile strength $f_{Utu,cal}$. The fiber efficiency μ_1 is determined using the relation between $\mu_{0,y}$ and μ_1 (Bastien-Masse et al.). $f_{Utu,cal}$ is calculated using equation (1). $f_{Ute,cal}$ is calculated using the proposed model explained in section 2.2.

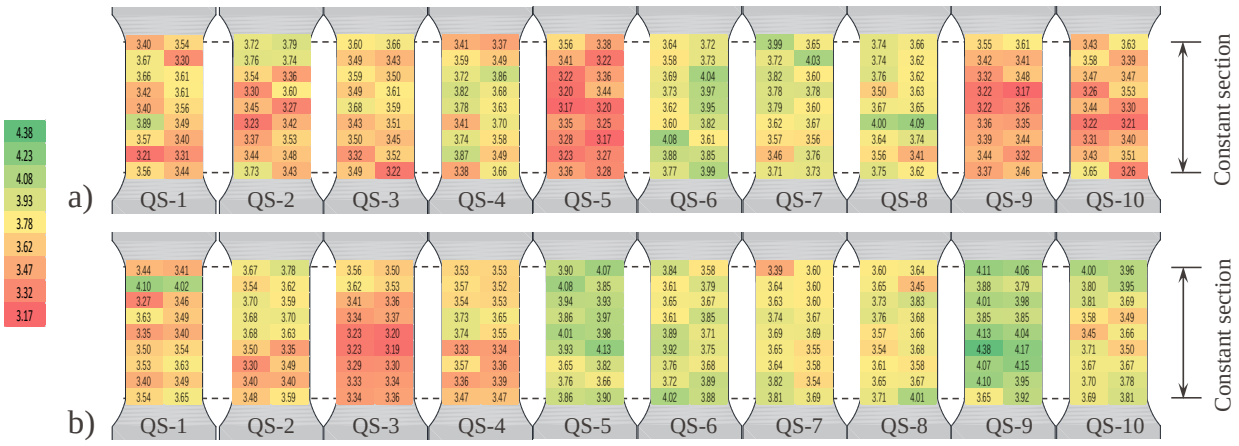

Figure 5 Local fiber volume V_f: a) casting surface; b) sheathed surface (unit: %)

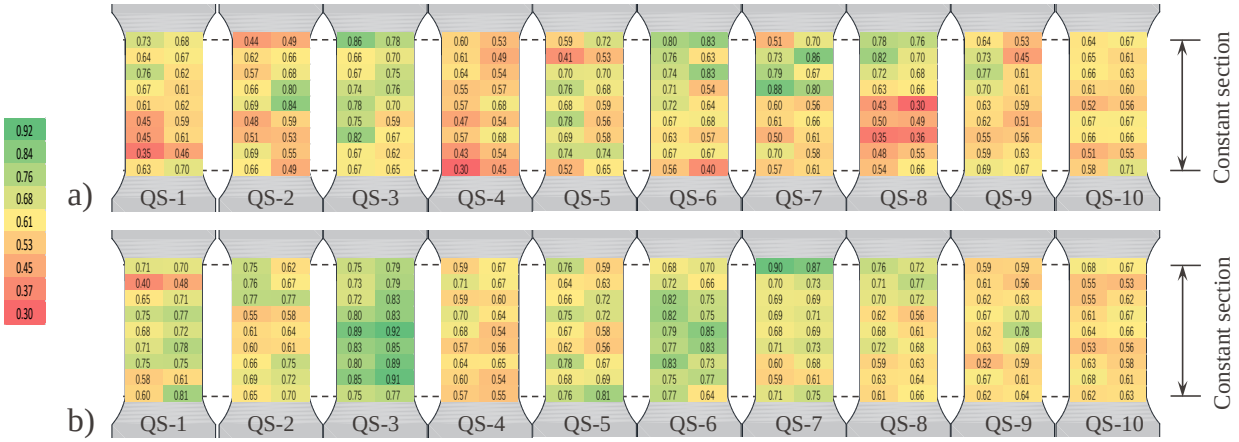

Figure 6 Local fiber orientation $\mu_{0,y}$: a) casting surface; b) sheathed surface

Table 2 Local fiber distribution and tensile features

Reference	Specimen	V_f (%)	$\mu_{0,y}$	μ_1	ε_{Ute} (‰)	ε_{Utu} (‰)	f_{Utu} (MPa)	f_{Ute} (MPa)	$f_{Ute,cal}$ (MPa)	$f_{Utu,cal}$ (MPa)
Present study	QS-1	3.52	0.64	0.95	0.19	>0.40**	11.72	9.31	8.88	12.17
	QS-2	3.53	0.64	0.95	0.20	0.75	10.97	9.18	8.91	12.21
	QS-3	3.43	0.76	0.98	0.22	0.65	13.74	10.95	10.24	14.53
	QS-4	3.56	0.58	0.94	0.20	>1.5	10.88*	9.49	8.16	11.04
	QS-5	3.60	0.66	0.96	0.23	>1.5	11.84*	10.59	9.36	12.97
	QS-6	3.78	0.71	0.97	0.25	>1.5	13.90*	11.66	10.56	14.81
	QS-7	3.68	0.69	0.96	0.20	>0.70**	11.48	10.00	9.99	13.86
	QS-8	3.68	0.62	0.95	0.21	>1.5	11.51*	9.66	9.00	12.33
	QS-9	3.69	0.62	0.95	0.20	>1.5	10.39*	9.05	9.03	12.36
	QS-10	3.57	0.62	0.95	0.21	1.23	11.15	10.33	8.73	11.96
(Shen and Brühwiler)	T1-1	3.8	0.68	0.98	0.23	3.84	12.85	9.96	9.30	13.17
	T1-2		0.62	0.95	0.22	0.71	11.55	9.87	8.50	11.64
	T1-3		0.53	0.92	0.19	2.67	9.62	8.20	7.30	9.63
	T1-4		0.53	0.92	0.21	0.88	9.80	8.62	7.30	9.63
	T1-5		0.52	0.91	0.18	0.33	9.49	8.10	7.16	9.35

** f_{Utu} is not reached before unloading. The maximum stress at the strain of 1.5 ‰ is used.*
***: Fracture occurs beyond the measurement range of LVDT.*

As shown in Table 2 and Figures 5 and 6, the average V_f of specimens QS-1 to 10 are from 3.43% to 3.78%, close to the recipe value 3.42%. The average $\mu_{0,y}$ of QS-1 to 10 are from 0.58 to 0.76. For each specimen, the sheathed surface has lower average $\mu_{0,y}$ than that of the casting surface and the lowest $\mu_{0,y}$ are found on the casting side.

Figure 7 and Table 2 show the stress-strain curves of QS-1 to 10 from the test beginning up to the strain of 1.5‰ and the corresponding tensile features, respectively. All specimens exhibit strain hardening behavior. The values of elastic limit f_{Ute} ranges from 9.05 MPa to 11.66 MPa with the

corresponding strain ranging from 0.19 ‰ to 0.25 ‰. The tensile strength of specimens QS-1 to 3, 7 and 10 are respectively 11.72 MPa, 10.97 MPa, 13.74 MPa, 11.48 MPa and 11.15 MPa, while the strain ε_{Utu} are over 0.4‰, 0.75‰, 0.65‰, over 0.7‰ and 1.23‰. Specimens QS-4 to 10 are loaded to the strain of 1.5‰ and unloaded. Because the stress levels of QS-4 to 6 and QS-8 and 9 have the increasing trend before unloading, their strains at tensile strength ε_{Utu} could be larger than 1.5‰ and their tensile strengths f_{Utu} could be larger than the maximum stresses reached during loading, which are 10.88 MPa, 11.84 MPa, 13.90 MPa, 11.51 MPa and 10.39 MPa, respectively.

Figure 8 and Table 2 show the experimental and calculated results of elastic limit and tensile strength obtained from the present study and (Shen and Brühwiler). The calculated tensile strengths $f_{Utu,cal}$ are all close to the experimental results f_{Utu} with difference ranging from 0.01 MPa to 2.38 MPa. The calculated elastic limits $f_{Ute,cal}$ are close to, while all slightly higher than the experimental results $f_{Ute,cal}$ with difference ranging from 0.01 MPa to 1.6 MPa. This shows that the elastic limit of UHPFRC has a linear relation with the average fiber orientation for orientation coefficients between 0.5 and 0.8 and can be appropriately estimated using the proposed model.

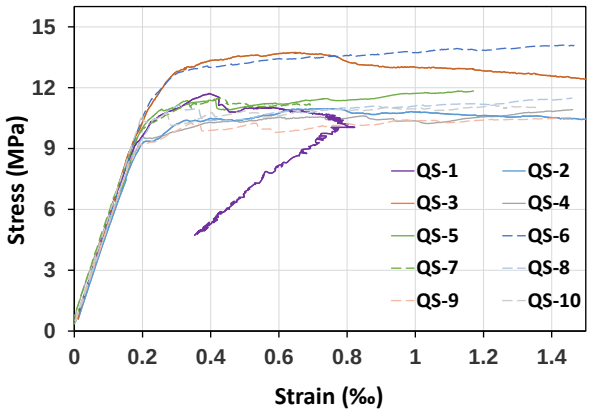

Figure 7 Stress-strain diagram of ten tensile tests

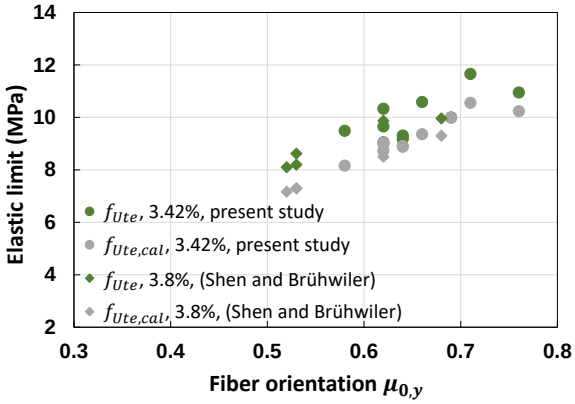

Figure 8 Fiber orientation and elastic limit from calculation and tests

5. Conclusions

Based on ten uniaxial tensile tests and literature data, this paper discusses the influence of fiber orientation on the elastic limit tensile stress of UHPFRC. The following conclusions are obtained:

- Analysis of experimental results from three independent research works show that the fiber orientation has significant influence on the matrix tensile strength of UHPFRC, while this parameter is not explicitly considered by current estimation model of the elastic limit.
- An original model relating the fiber orientation to the elastic limit is proposed based on literature data.
- The results of local fiber distribution and elastic limit from 15 tensile tests show that the proposed model can appropriately estimate the elastic limit of UHPFRC.

6. References

- Bastien-Masse, M. et al., "Effect of Fiber Orientation on the In-Plane Tensile Response of UHPFRC Reinforcement Layers." Cement and Concrete Composites, vol. 67, 2016, pp. 111–25.
- Denarié E. et al., Characterization of the Tensile Response of Strain Hardening UHPFRC — Chillon Viaducts. 2017.
- Habel K. et al., "Development of the Mechanical Properties of an Ultra-High Performance Fiber Reinforced Concrete (UHPFRC)." Cement and Concrete Research, vol. 36, no. 7, 7, July 2006, pp. 1362–70. DOI.org (Crossref), https://doi.org/10.1016/j.cemconres.2006.03.009.
- Mohamed Abdul H. and Denarié E., "Tensile Response of UHPFRC under Very Low Strain Rates and Low Temperatures." Cement and Concrete Research, vol. 133, July 2020, p. 106067. ScienceDirect, https://doi.org/10.1016/j.cemconres.2020.106067.
- Helbling, A. and Brühwiler E., "Eine neue Halterung für Zugversuche mit Beton-Probekörper." Material und Technik, vol. 4, 1987, pp. 103–07.
- Inglis, C. E., "Stresses in a Plate Due to the Presence of Cracks and Sharp Corners." Trans Inst Naval Archit, vol. 55, 1913, pp. 219–41.
- Martinie, L. and Roussel N., "Simple Tools for Fiber Orientation Prediction in Industrial Practice." Cement and Concrete Research, vol. 41, no. 10, Oct. 2011, pp. 993–1000. ScienceDirect, https://doi.org/10.1016/j.cemconres.2011.05.008.
- Maya Duque, L. F. and Graybeal B., "Fiber Orientation Distribution and Tensile Mechanical Response in UHPFRC." Materials and Structures, vol. 50, no. 1, Feb. 2017, p. 55. DOI.org (Crossref), https://doi.org/10.1617/s11527-016-0914-5.
- Naaman, A. E., A Statistical Theory of Strength for Fiber Reinforced Concrete. Massachusetts Institute of Technology, 1972.
- Naaman, A. E., "High Performance Fiber Reinforced Cement Composites." Naaman AE. High-Performance Construction Materials: Science and Applications. Singapore: World Scientific Publishing, 2008, pp. 91–153.
- Nunes, S. et al., "Estimation of the Tensile Strength of UHPFRC Layers Based on Non-Destructive Assessment of the Fibre Content and Orientation." Cement and Concrete Composites, vol. 83, 2017, pp. 222–38.
- Oesterlee, C., "Structural Response of Reinforced UHPFRC and RC Composite Members." Infoscience, THESIS, EPFL, 2010, https://doi.org/10.5075/epfl-thesis-4848.
- Shen, X. J. and Brühwiler E., "Influence of Local Fiber Distribution on Tensile Behavior of Strain Hardening UHPFRC Using NDT and DIC." Cement and Concrete Research, vol. 132, June 2020, p. 106042. ScienceDirect, https://doi.org/10.1016/j.cemconres.2020.106042.